Since January 2020 Elsevier has created a COVID-19 resource centre with free information in English and Mandarin on the novel coronavirus COVID-19. The COVID-19 resource centre is hosted on Elsevier Connect, the company's public news and information website.

Colloids and Surfaces A: Physicochemical and Engineering Aspects 656 (2023) 130393

Contents lists available at ScienceDirect

Colloids and Surfaces A: Physicochemical and Engineering Aspects

journal homepage: www.elsevier.com/locate/colsurfa

Buchwald–Hartwig coupled conjugated microporous polymer for efficient removal COVID-19 antiviral drug famciclovir from waters: Adsorption behavior and mechanism

Hai-Chen Tu, Ling-Xi Zhao *, Lu Liu, Xiao-Xing Wang, Jin-Ming Lin, Xia Wang *, Ru-Song Zhao

Qilu University of Technology (Shandong Academy of Sciences), Shandong Analysis and Test Center, Key Laboratory for Applied Technology of Sophisticated Analytical Instruments of Shandong Province, Jinan 250014, China

HIGHLIGHTS

- BPT-BZ-CMP was synthesized and used to adsorb FCV for the first time.
- The adsorption capacity of BPT-BZ-CMP was the best and reached 347.8 mg/g.
- The hydrogen bonding, π-π and C-H···π interactions enhanced the adsorption of FCV.
- BPT-BZ-CMP had excellent regeneration ability to be an outstanding sorbent.

GRAPHICAL ABSTRACT

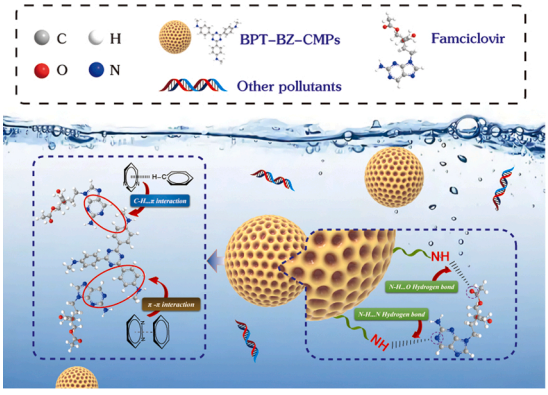

ARTICLE INFO

Keywords:
Conjugated microporous polymer
Famciclovir
Adsorption
Mechanism

ABSTRACT

The consumption of famciclovir (FCV) has been increased dramatically since the outbreak of coronavirus in 2019, and the pollution and harm of FCV in waters are concerned. Here, by utilizing aryl halides on 2, 4, 6-tris(4-bromophenyl)– 1, 3, 5-triazine (BPT) and primary amine groups on benzidine (BZ), a novel conjugated microporous polymer, namely BPT-BZ-CMP, was synthesized by Buchwald–Hartwig coupling reaction and applied in the removal of FCV from aqueous solution firstly. The synthesized BPT-BZ-CMP were characterized by various methods, including FTIR, SEM, BET, and Zeta–potential. Due to the micropore structure and high specific surface area, it took only 30 min for BPT-BZ-CMP to adsorb FCV to reach an equilibrium, and the maximum adsorption capacity was 347.8 $mg \cdot g^{-1}$. The Liu and pseudo-second-order kinetic models properly fit the adsorption equilibrium and kinetic data, respectively. The adsorption process was a spontaneous process, and the hydrogen bonding, π–π interaction and C–H···π interaction enhanced the adsorption of FCV on BPT-BZ-CMP. BPT-BZ-CMP maintained a good adsorption capacity after four consecutive adsorption–desorption cycle experiments. This study confirmed the potential of BPT-BZ-CMP as efficient sorbent to remove FCV from aqueous solutions.

* Corresponding authors.
E-mail addresses: lingxi0716@163.com (L.-X. Zhao), xia-w21cn0@163.com (X. Wang).

https://doi.org/10.1016/j.colsurfa.2022.130393
Received 8 August 2022; Received in revised form 30 September 2022; Accepted 16 October 2022
Available online 18 October 2022

1. Introduction

The emergence of drugs in waterbodies was reported in the United States as early as the 1970 s [1]. The residues of antiviral drugs easily flow into waterbodies because of their low biodegradability, and they constitute chronic toxicity to aquatic organisms in natural waterbodies and harm humans through bioaccumulation amplification [2]. One of the antiviral drugs, famciclovir (FCV), is a ring-opening nucleoside drug mainly used to treat herpes virus infections [3]. Owing to the global presence of COVID-19, FCV was proposed as an add-on therapy after the onset of the coronavirus disease 2019 (COVID-19) along with COVID-19 treatments [4], the environmental harm caused by the large-scale use and bioaccumulation of FCV is evident. Therefore, removing FCV from waterbodies should be promptly tackled.

Adsorption is an attractive candidate for the removal of antiviral drugs because of its economic feasibility, environmental friendliness, and simple operation [5–7]. Meanwhile, to achieve efficient adsorption, sorbents with high capacity and fast rate are required. Many sorbents have been utilized for adsorption, such as carbon nanotubes[8], nanofibers [9], powdered activated carbon [10], metal-organic frameworks [11], covalent organic frameworks [12], etc. Advanced materials as sorbents with excellent adsorption capacity and regeneration have garnered substantial attention.

Porous materials exhibit great potential as sorbents because of their high specific surface area and limited pore space [13–15]. Of which, the unique surface wettability and excellent selective adsorption properties of conjugated microporous polymers (CMPs) make them show potential application prospects as high-efficiency adsorbents in the field of waterbodies treatment. After the first synthesis of CMPs by Cooper's group [16], CMPs have been continuously developed and innovated in terms of design and synthesis, and they have demonstrated great potential in gas storage [17], separation [18], sensing[19], catalysis [20, 21], and batteries[22]. The generation of C-N bonds in the polymer network by palladium-catalyzed cross-coupling of arylamines with aryl halides is the mainstay of the synthesis of N-containing CMPs by the Buchwald-Hartwig (BH) coupling method, and can obtain covalent bonds with high chemical stability, which is a great advantage for a sorbent[23–25].

Here, a stable CMP (BPT-BZ-CMP) with a high surface area was prepared from 2, 4, 6-tris(4-bromophenyl)– 1, 3, 5-triazine (BPT) and benzidine (BZ) by the BH coupling reaction, for use as a sorbent for the effective removal of FCV from aqueous solutions. Batch adsorption performances were systematically analyzed through kinetic and thermodynamic studies. The influencing factors (pH and sorbent concentration) were tested, and recycling experiments were investigated to evaluate the environmental application potentials of BPT-BZ-CMP. In

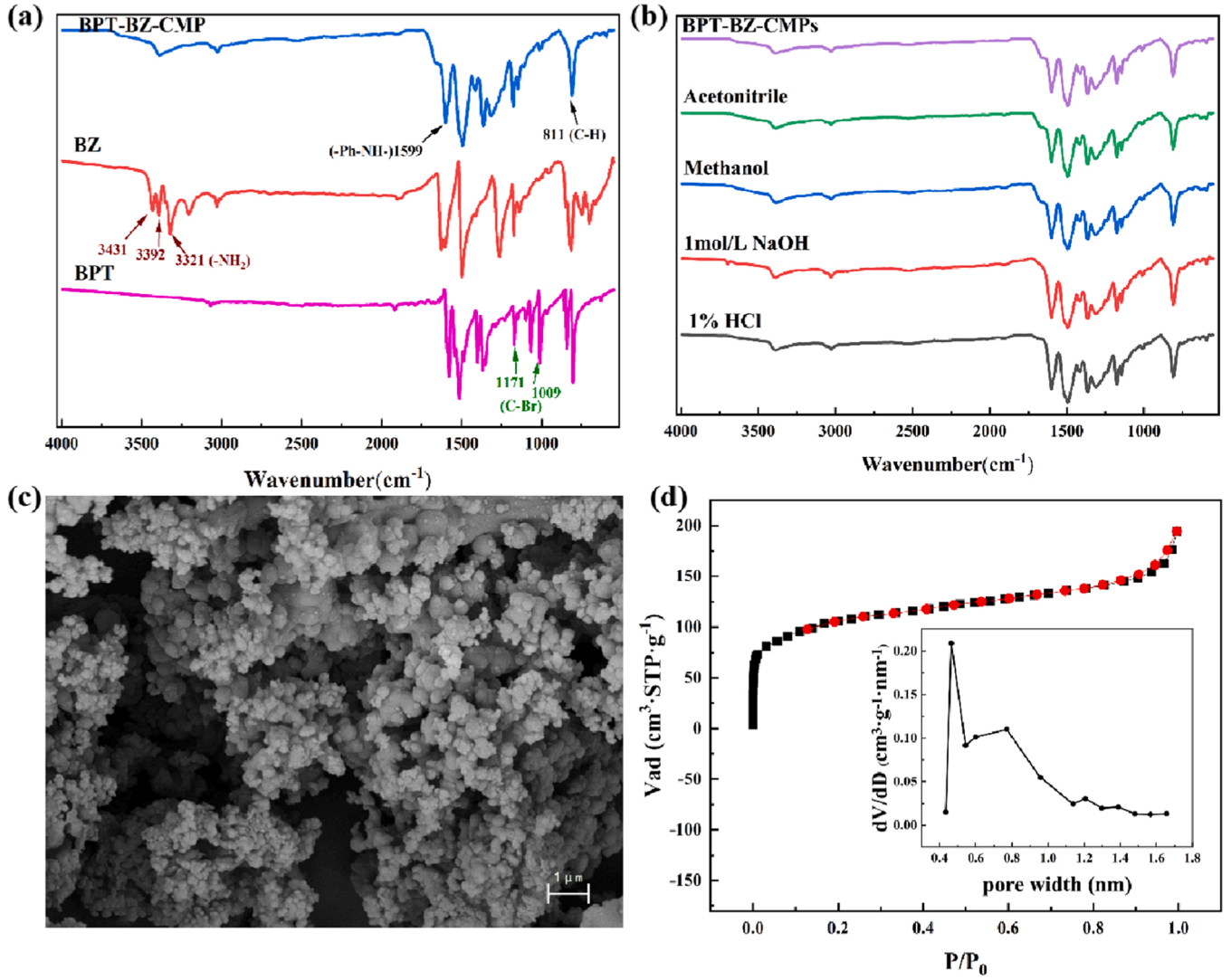

Fig. 1. FT-IR spectra of BPT-BZ-CMP in material synthesis (a) and stability experiments (b), SEM micrograph (c), N_2 adsorption–desorption isotherms and pore-size distribution of BPT-BZ-CMP (d).

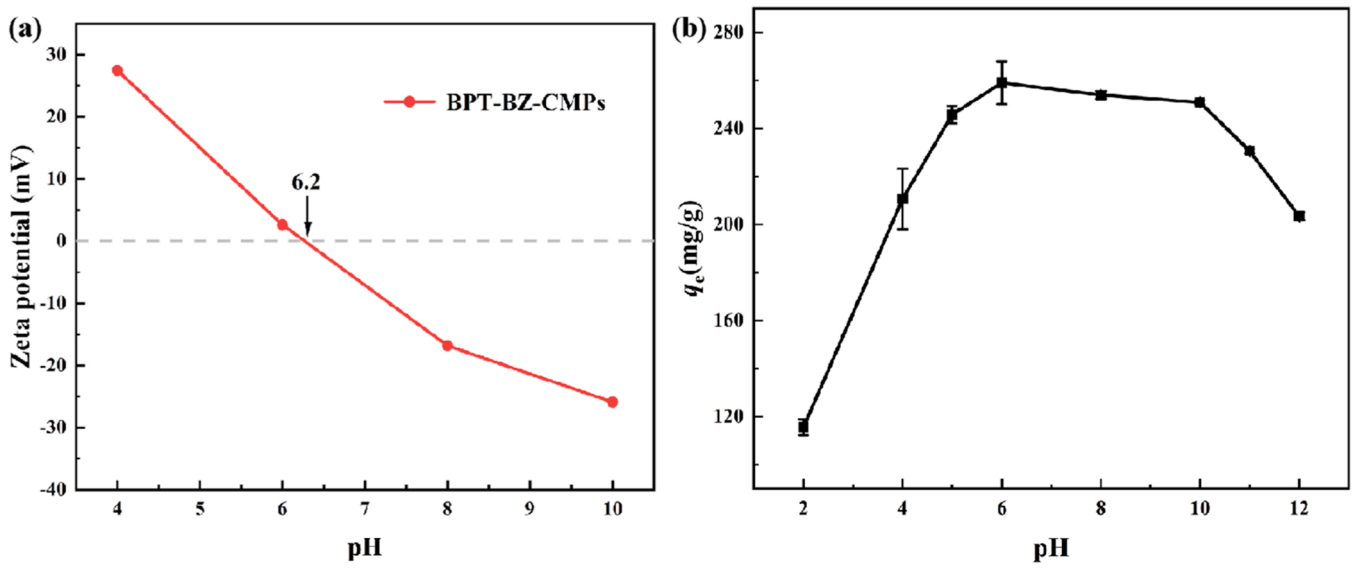

Fig. 2. Zeta-potential of BPT-BZ-CMP (a) and pH influence (C_s = 0.5 g·L^{-1}, T = 308 K) for FCV adsorption on BPT-BZ-CMP (b).

addition, the adsorption mechanism was explored by Fourier transform infrared (FT-IR) spectroscopy, X-ray photoelectron spectroscopy (XPS), and density functional theory (DFT) calculations. This study provides a novel method for FCV removal based on BPT-BZ-CMP for practical water remediation and elucidates the adsorption mechanism.

2. Material and methods

2.1. Chemicals and characterization

BPT, BZ, Bis(dibenzylideneacetone)palladium (Pd[dba]$_2$), and 2-(dicyclohexylphosphino)− 2,4,6-tri-i-propyl-1,1-biphenyl (XPhos) were obtained from Alpha Bio Co., Ltd. (Tianjin, China). Sodium tert-butoxide (NaOtBu) and FCV were purchased from Aladdin Biochemical Technology Co., Ltd. (Shanghai, China). An FCV stock solution (1000 mg·L^{-1}) was prepared with purified water.

Scanning electron microscopy (SEM, SUPPATM 55, Zeiss, Germany) was employed to observe the morphology and size of the BPT-BZ-CMP material. FT-IR (Nicolet 710 infrared) was employed to record the functional groups of the material at wavelengths in the range of 500–4000 cm^{-1}. The surface area of BPT-BZ-CMP was determined by JW-BK300C volumetric sorption analyzer. The XPS spectra were recorded by Thermo Fisher Escalab 250 Xi system.

2.2. Preparation of BPT-BZ-CMP

This study polymerized BPT-BZ-CMP in an optimized manner according to previously reported methods [26]. BPT (360.4 mg), BZ (184.2 mg), Pd(dba)$_2$ (34.5 mg,), XPhos (42.9 mg), and NaOtBu (672.7 mg) were added in a round bottom flask under a nitrogen atmosphere. Thereafter, 1,4-dioxane (60 mL) was added to the mixture and heated to 85 °C with stirring. After 24 h, the reaction was cooled to room temperature, and the solvents were removed by filtration (Fig. S1). The remaining solid was washed with purified water (50 mL) and four times with methanol (200 mL). The product was dried at 60 °C under vacuum conditions for 24 h to obtain BPT-BZ-CMP.

2.3. Adsorption experiments

For the adsorption kinetics experiments, a weighed sample of BPT-BZ-CMP was added into a 200 mg·L^{-1} FCV aqueous solution (pH = 6.0), sonicated in ultrasound for 10 s, and shaken at 308 K. The supernatant of the dispersion was filtered through a 0.45 μm syringe filter at different times. For the adsorption isotherm and thermodynamic experiments, the BPT-BZ-CMP samples were dispersed in FCV (volume, 10 mL; concentration, 0–350 mg·L^{-1}) and shaken at 288, 298, 308, and 318 K for 12 h. The absorbance was detected at 305 nm with an ultraviolet spectrophotometer, and the concentration of the supernatant was determined. The amount of FCV adsorbed by BPT-BZ-CMP was get by subtracting the mass of FCV in the treated solution from the mass of FCV in the initial solution using Eqs. (S1) and (S2).

2.4. DFT

DFT calculations were employed to simulate the adsorption mechanism with the Dmol^3 program package in Material studio. The exchange-correlation energy was calculated by the Perdew–Burke–Ernzerhof function within the generalized gradient approximation. The c-axis of the one-layer-four-hole slab with a 3 × 2 × 1 BPT-BZ-CMP supercell was built to adsorb five identical FCV molecules. The guest molecular adsorption was analyzed by the Metropolis Monte Carlo algorithm.

3. Results and discussion

3.1. Characterization of BPT-BZ-CMP

The FT-IR spectra (Fig. 1a) showed that the original characteristic peaks centered at 3321, 3392, and 3431 cm^{-1} correlating with the amine groups of BZ (–NH$_2$ stretching) and the aromatic C–Br stretching vibrations at 1171 and 1009 cm^{-1} arising from the aromatic C–Br groups of BPT were strongly attenuated in the BPT-BZ-CMP spectra. This indicated that the two monomers were combined to form the BPT-BZ-CMP network via BH coupling successfully. Concomitantly, the –PH–NH– (1599 cm^{-1}) and aromatic C–H (811 cm^{-1}) bands corresponding to the benzenoid rings were observed, which confirmed the successful synthesis of BPT-BZ-CMP[27]. Solid-state ^{13}C cross-polarization magic-angle spinning (CP/MAS) NMR technique can be well used to investigate the structure of insoluble polymeric material BPT-BZ-CMP (Fig. S2). The spectra of BPT-BZ-CMP show two main resonances at 147 and 116 ppm, which were assigned to the substituted phenyl carbons and unsubstituted phenyl carbons, respectively. A peak at 170 ppm was assigned to the triazine carbon of CMP. Signals derived from the phenyl groups of the triazine unit were observed at 127, 130 and 139 ppm.

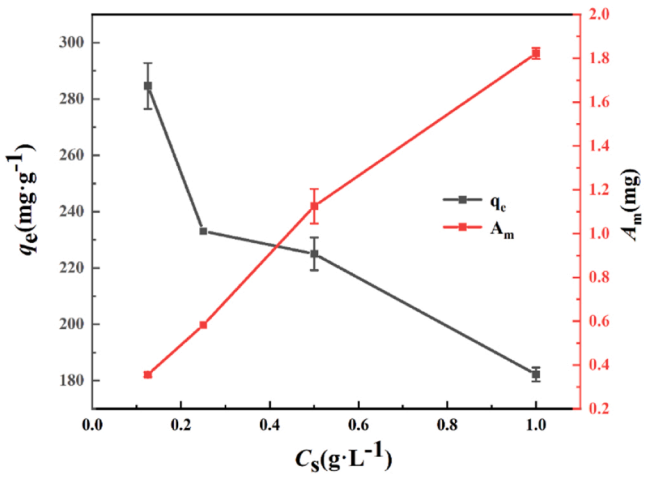

Fig. 3. The effect of sorbent concentration (pH = 6.0, T = 308 K).

The chemical stability of BPT-BZ-CMP as a new FCV sorbent is important. Fig. 1b shows the FT-IR spectra of BPT-BZ-CMP after 48 h in different organic solvents, including methanol, acetonitrile, 1 mol·L^{-1} NaOH, and 1% HCl. There was no significant change in each spectrum, indicating that BPT-BZ-CMP had high chemical stability. The thermogravimetric analysis (TGA) of BPT-BZ-CMP under Ar (Fig. S3) showed that the material was stable up to 200 °C and yielded > 85 wt% chars when heated to 700 °C. The better thermal stability of BPT-BZ-CMP is attributed to the multiple stable C-N bonds in its structure, forming highly cross-linked network structures.

As shown in Fig. 1c, BPT-BZ-CMP exhibited uneven particulate-like morphologies with nanoparticle diameters in the range of 100–500 nm. The adsorption performance was closely related to the specific surface area and pore structure of the sorbent. Noteworthily, BPT-BZ-CMP exhibited a large specific surface area of 368 m^2·g^{-1}. This was calculated from the Langmuir adsorption isotherm equation [Eq. (S3)]. This large specific surface area was quite beneficial for the adsorption performance. And the Elemental mapping of SEM confirmed the presence of C and N atoms in BPT-BZ-CMP materials (Fig. S4). The N_2 adsorption-desorption behavior of BPT-BZ-CMP (Fig. 1d) was Type I, reflecting the pore-filling phenomenon of a microporous sorbent. The median pore width distribution of BPT-BZ-CMP was 0.6825 nm. The large surface area and micropore structure provided additional adsorption spots to improve the FCV adsorption efficiency and rate.

3.2. Effects of pH and sorbent concentration

Here, the effect of pH on the adsorption of BPT-BZ-CMP was investigated at a temperature of 308 K and an FCV concentration of 200 mg·L^{-1} in the pH range of 2.0–12.0. As shown in Fig. 2b, BPT-BZ-CMP exhibited a poor adsorption effect on FCV at a pH of 2 because of the instability of FCV in a strong-acid environment. The surface charge property of BPT-BZ-CMP was determined by measuring the zeta potentials in the pH range of 4.0–10.0 (Fig. 2a). The pH at the point of zero charge (pH_{PZC}) of BPT-BZ-CMP was 6.2. When pH < 6.2, the superficial charge of BPT-BZ-CMP was positive, but it became negative when pH > 6.2[28]. The pKa of FCV was 4.0, indicating that FCV was in anion form at pH > 4.0. Hence, the high FCV removal efficiency mainly occurred via hydrogen bond interaction, not electrostatic force within a pH range of 5.0–10.0. When the pH decreased, the free hydrogen ions increased and covered the negative atoms, resulting in a decrease in hydrogen bonds. Conversely, the number of hydroxides in the solution increased, and there were only a few free hydrogen ions to form abundant hydrogen bonds as the pH increased. Therefore, excess acid or base was not conducive for the formation of hydrogen bonds between the two compounds. Thus, the interaction between BPT-BZ-CMP and FCV gradually weakened while the π–π interaction responded to the adsorption in view of a certain adsorption capacity at pH of 4.0 and 10.0–12.0.

The concentration of the sorbent is an important factor affecting the adsorption. However, economic factors should be examined when considering the adsorption effect. Therefore, when determining the amount of sorbent, it was necessary to ensure the removal effect and cost-effectiveness. As shown in Fig. 3, the total removal amount (A_m) of FCV increased from 0.356 to 1.822 mg, but the equilibrium adsorption amount (q_e) decreased from 284.6 to 182.2 mg·g^{-1} with the concentration of the sorbent (C_s) changing from 0.125 to 1.0 g·L^{-1}. The high q_e at low BPT-BZ-CMP doses may be due to the complete exposure of the adsorption sites, and the surface adsorption saturation rate was rapid. The adsorption capacity decreased with an increase in BPT-BZ-CMP dosage, owing to the uncovered adsorption sites. This phenomenon was known as the C_s effect [29]. Therefore, economically, the optimal concentration of BPT-BZ-CMP should be 0.50 g·L^{-1} as the optimal choice.

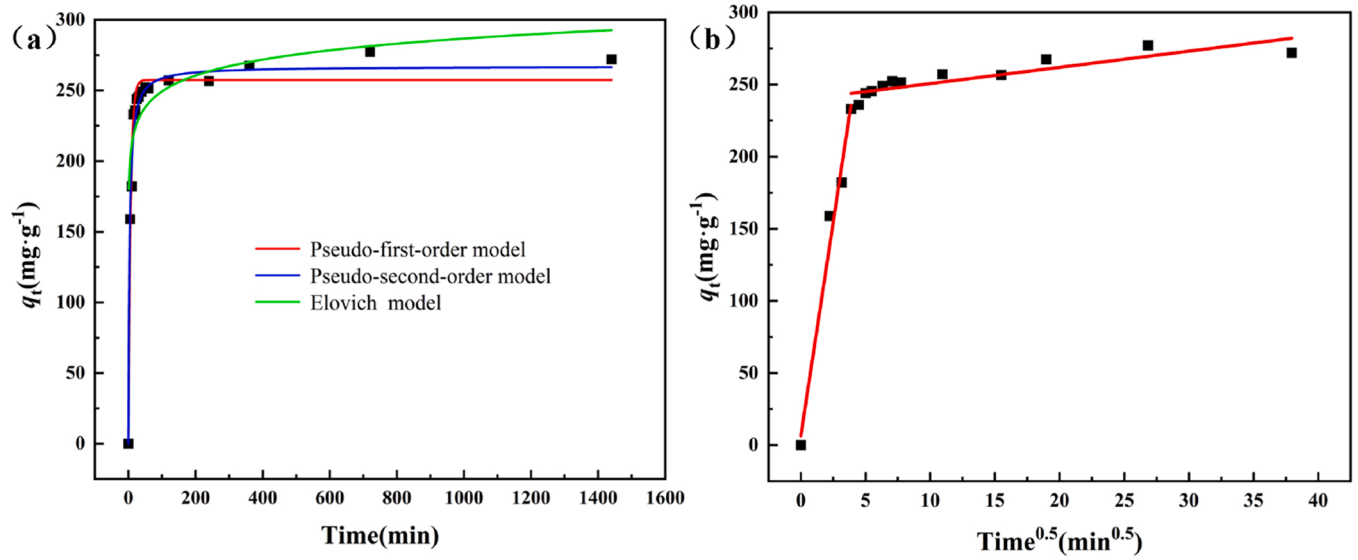

Fig. 4. Adsorption kinetics fitted by pseudo-first-order, pseudo-second-order and Elovich models (a), and intra-particle diffusion model (b).

Table 1
Parameters of kinetic equations for FCV adsorption onto BPT-BZ-CMP.

Kinetic model	Parameter	Value
Pseudo-first-order	q_e (mg·g^{-1})	257.4
	k_1 (min^{-1})	0.151
	R^2	0.9723
Pseudo-second-order	q_e (mg·g^{-1})	267.0
	k_2 (g·mg^{-1}min^{-1})	0.001
	R^2	0.9866
Elovich	α (mg·g^{-1}min^{-1})	7.25×10^5
	β (g·mg^{-1})	0.061
	R^2	0.9332

3.3. Adsorption kinetics

Adsorption kinetic experiments were performed to study the nature of the adsorption process and adsorption mass transfer process. As shown in Fig. 4a, pseudo-first-order [Eq. (S4)], pseudo-second-order [Eq. (S5)], and Elovich models [Eq. (S6)] were employed to fit the experimental data, and the parameters are listed in Table 1. The results showed that FCV quickly reached the adsorption equilibrium within about 30 min at the initial FCV concentration of 200 mg·L^{-1} and pH of 6.0 at 308 K. This indicated that BPT-BZ-CMP could efficiently remove FCV at an extremely high adsorption speed. The correlation coefficients (R^2) of the three models were 0.9723, 0.9866, and 0.9332, respectively. From the values of R^2, the pseudo-second-order model obtained the best fit, which implied that the adsorption process was mainly controlled by chemical action, rather than mass transfer.

It was difficult to confirm the potential rate-controlled steps of the adsorption process using only the aforementioned models. Hence, intraparticle diffusion was considered to fit the obtained experimental results, which were calculated by Eq. (S7) [30]. Fig. 4b shows that the diffusion process followed two steps. The slower second step controlled the main rate process, demonstrating that the adsorption process occurred through surface and intraparticle diffusion [31,32].

3.4. Adsorption isotherm

The adsorption isotherms allowed the visualization of important information when investigating the q_m and explaining the adsorption properties of the adsorbate bound to the surface of the sorbent[33–37]. The equilibrium data were analyzed using the Langmuir [Eq. (S8)], Freundlich [Eq. (S9)], and Liu [Eq. (S10)] models, and the nonlinear fitting curves are shown in Fig. 5. Table 2 summarizes the constants and R^2 values obtained from the aforementioned three isotherm models applied for the adsorption of FCV on BPT-BZ-CMP.

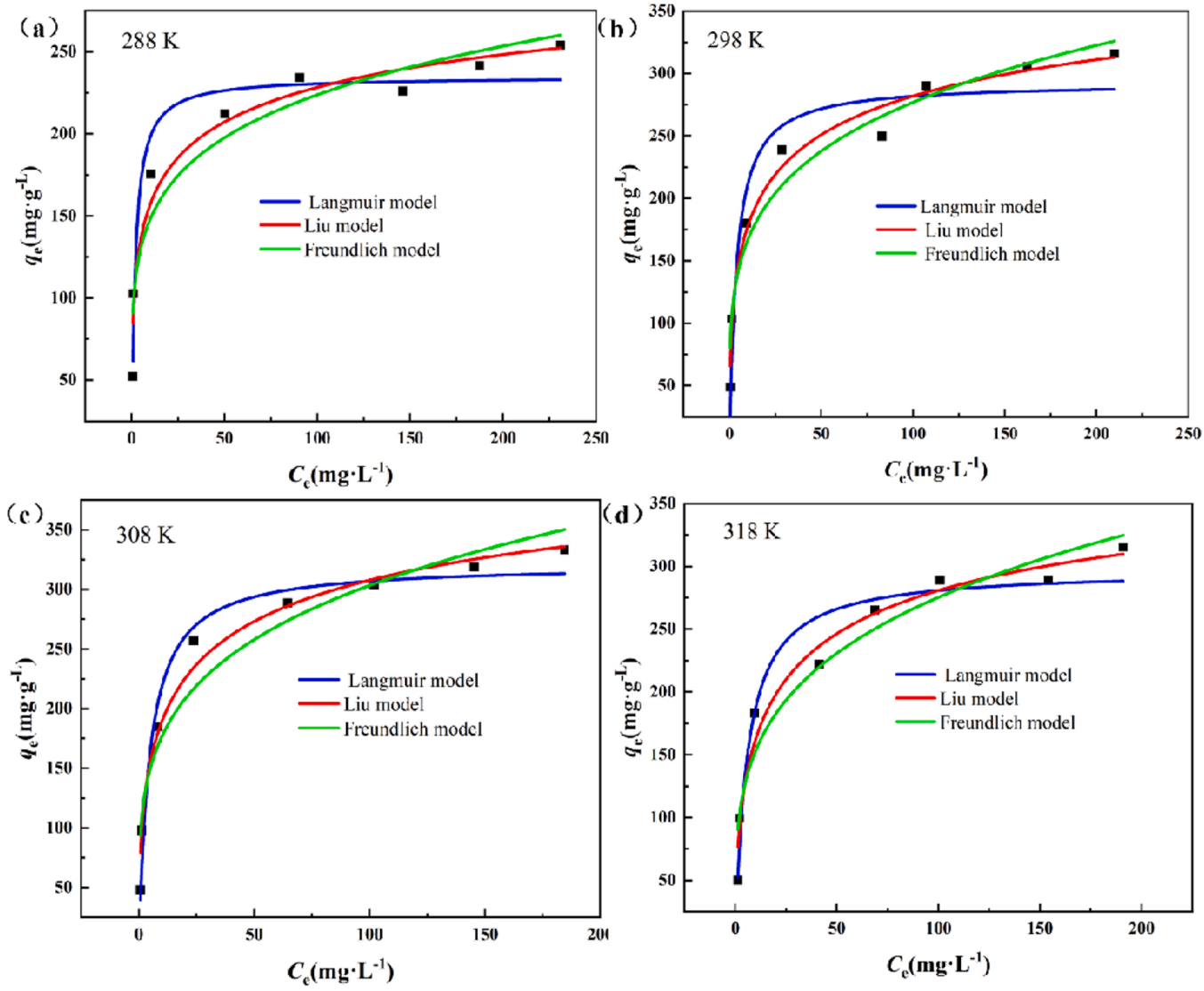

Fig. 5. Adsorption isotherms fitted by Langmuir, Freundlich, and Liu models at 288 (a), 298 (b), 308 (c), and 318 K (d) (C_s = 0.5 g·L^{-1}, pH = 6.0).

Table 2
Parameters of adsorption isotherm equations for FCV on BPT-BZ-CMP.

Adsorption isotherm	Parameter	Temperature (K)			
		288	298	308	318
Langmuir	q_m (mg·g^{-1})	234.8	292.5	321.3	297.1
	K_L (L·mg^{-1})	0.54	0.26	0.21	0.17
	R^2	0.9482	0.9287	0.9748	0.9573
Freundlich	K_F [mg·g^{-1}·(mg·L^{-1})$_F^{-1/n}$]	97.9	100.7	103.2	85.2
	n_F	5.58	4.55	4.27	3.93
	R^2	0.9206	0.9625	0.9414	0.9468
Liu	K_g (L·mg^{-1})	0.04	0.03	0.04	0.04
	n_L	2.99	2.50	2.27	2.01
	R^2	0.9530	0.9829	0.9803	0.9738

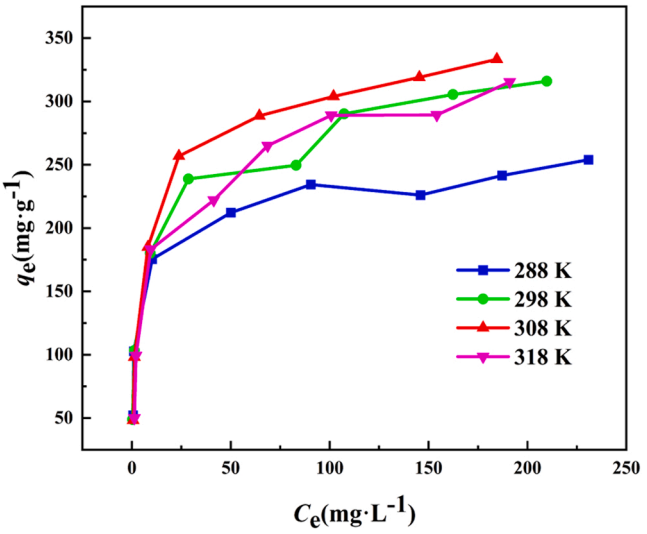

Fig. 6. Effect of temperature on the adsorption of FCV by BPT-BZ-CMP (C_s = 0.5 g·L^{-1}, pH = 6.0).

The Langmuir model assumed that adsorption only occurred at local sites and the same adsorption energy exists in all the adsorption sites. The equilibrium constant, K_L, indicates whether the adsorption process is unfavorable, linear, favorable, or irreversible, $K_L > 1$, $K_L = 1$, $0 < K_L < 1$ and $K_L = 0$, respectively. The K_L values were 0.5398, 0.2610, 0.2136, and 0.1706 L·mg^{-1} at different temperatures (Table 2), revealing that the adsorption process was favorable [38].

The Freundlich model is an empirical equation describing multilayer adsorption on inhomogeneous surfaces. The magnitude of the Freundlich constant (n_F) indicates whether the adsorption process is favorable ($n_F > 1$) or chemisorption ($n_F < 1$). The n_F values were 5.58, 4.55, 4.27, and 3.93 (Table 2), which confirmed that the adsorption of FCV by BPT-BZ-CMP was a favorable process [39].

The Liu model assumed that the adsorption was heterogeneous. This was due to the existence of different active sites and different free adsorption energies acting simultaneously[40]. The Liu model afforded the highest R^2 values, which all exceeded 0.95. Therefore, the Liu model is the best isotherm model for the adsorption of FCV onto BPT-BZ-CMP [41,42].

3.5. Adsorption thermodynamics

Fig. 6 shows the effect of temperature (288–318 K) for FCV adsorption onto BPT-BZ-CMP. As shown, 308 K was the best adsorption temperature. Thermodynamic studies of the adsorption process by calculating thermodynamic parameters like Gibbs free energy (ΔG^O), enthalpy change (ΔH^O) and entropy change (ΔS^O) (Table 3). The thermodynamic equilibrium constant (K_e) was acquired by the Liu model's constant (K_g) [Eq. (S11)] [43,44]. The spontaneity of the adsorption of FCV onto BPT-BZ-CMP was based on the negative ΔG^Ovalue, which was calculated by Eq. (S12). Furthermore, ΔG^O decreased with an increase in temperature, indicating that the adsorption of FCV on BPT-BZ-CMP was endothermic [45,46]. The ΔH^O value calculated using Eq. (S13) was 1.59 kJ·mol^{-1}, which confirmed that the adsorption was an endothermic reaction. The positive $\Delta S^O$of 81.01 J·mol^{-1}·K^{-1} implied an increase in the stochasticity of the solid–liquid border, indicating the excellent attraction between BPT-BZ-CMP and FCV.

Table 3
Thermodynamic parameters for FCV adsorption onto BPT-BZ-CMP.

Temperature (K)	K_e (/)	ΔG^O (kJ·mol^{-1})	ΔH^O (kJ·mol^{-1})	ΔS^O (J·mol^{-1}·K^{-1})
288	9.5×10^3	-21.9	1.59	81.01
298	7.8×10^3	-22.2		
308	9.6×10^3	-23.5		
318	9.5×10^3	-24.2		

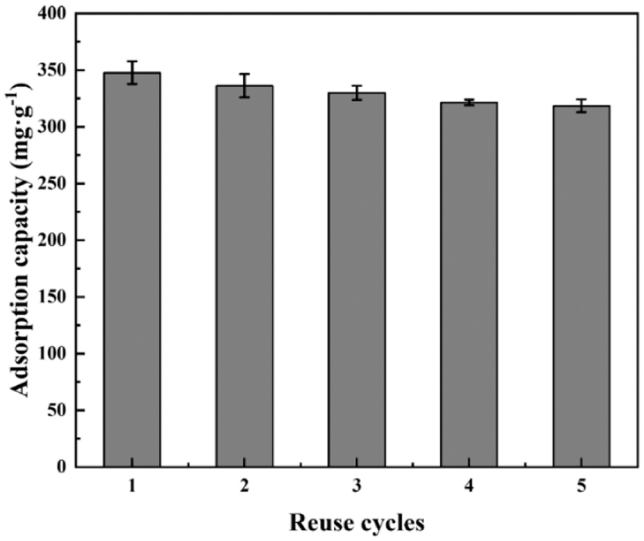

Fig. 7. FCV adsorption capacities by BPT-BZ-CMP after five recycle runs.

3.6. Regeneration of BPT-BZ-CMP

As an excellent sorbent in practical applications, the adsorption regeneration ability of BPT-BZ-CMP is crucial. Therefore, desorption and resorption experiments were performed to confirm its good regeneration ability. An acetonitrile solution containing ammonia (5%) was used to

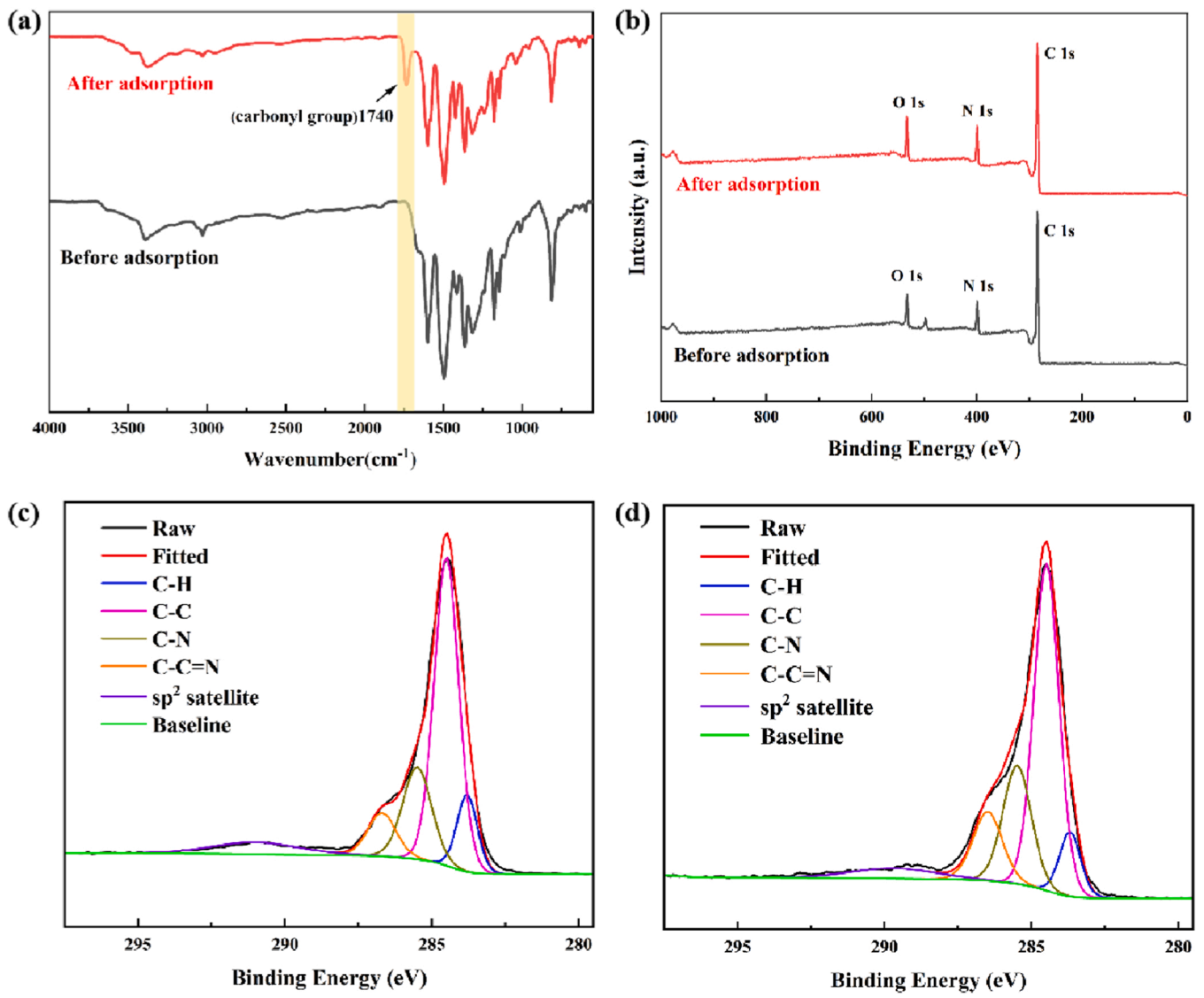

Fig. 8. FT-IR (a) and XPS spectra (b) of BPT-BZ-CMP prior to and after adsorption; and the XPS spectra of C1s prior to (c) and after (d) FCV adsorption by BPT-BZ-CMP.

desorb FCV from BPT-BZ-CMP. The recovery performance of BPT-BZ-CMP was investigated at an initial FCV concentration of 300 mg·L^{-1}, pH = 6.0, and T = 308 K using 5% ammonia-acetonitrile as the eluent. The adsorption capacity of BPT-BZ-CMP for four consecutive adsorption–desorption cycles is shown in Fig. 7. The adsorption capacity could reach 347.8 mg·g^{-1} initially, which was 336.2 mg·g^{-1} after the first desorption experiment and 330.0, 321.5, and 318.5 mg·g^{-1} for the three subsequent cycles, respectively. The adsorption capacity slightly decreased with an increase in the number of cycles, possibly due to incomplete elution of the desorption experiment, which prevented complete regeneration of the material. This performance confirmed the excellent adsorption regeneration ability of BPT-BZ-CMP for the removal of FCV and its feasibility as an outstanding sorbent for practical application.

3.7. Adsorption mechanism

Compared with the full FT-IR spectra of BPT–DMB–CMP prior to and after adsorption (Fig. 8a), a new characteristic peak at 1740 cm^{-1} ascribed to the carbonyl group of FCV appeared after adsorption, which revealed the successful adsorption of FCV by BPT-BZ-CMP. The XPS characterizations of BPT-BZ-CMP prior to and after FCV adsorption were analyzed and compared (Fig. 8b-d). The bond contents of C═C (284.5 eV) and C–N (285.5 eV) were significantly different in the C1s spectra of BPT-BZ-CMP after FCV adsorption (Table S1). These phenomena indicated π–π interaction between the aromatic ring of FCV and the benzene ring of BPT-BZ-CMP [47,48]. The bond ratio of C–C═N after adsorption was significantly higher than that before adsorption, which explained the successful adsorption of FCV by BPT-BZ-CMP.

DFT analysis was employed to confirm and reveal the interaction mechanism between FCV and BPT-BZ-CMP from a molecular structure perspective. The generalized gradient approximation (GGA) method with Perdew-Burke-Ernzerhof (PBE) function was employed to describe the interactions between core and electrons. For the binding energy and adsorption conformation simulations, the DFT-D functional to include the physical van der Waals interaction, which was demonstrated to be very important in the simulation of CMP adsorption. The force and energy convergence criterion were set to 0.002 Ha Å^{-1} and 10^{-5} Ha, respectively. Fig. 9a depicts the adsorption configuration of FCV adsorption on BPT-BZ-CMP. Some of the FCV molecules were accommodated in the hexagonal pore walls of BPT-BZ-CMP after adsorption. Fig. 9b and c demonstrate the possible π–π interactions and nonbond weak interactions among the benzene ring and C–H on BPT-BZ-CMP and the π-electron-rich aromatic ring of FCV, respectively. Hydrogen bonds were mainly generated

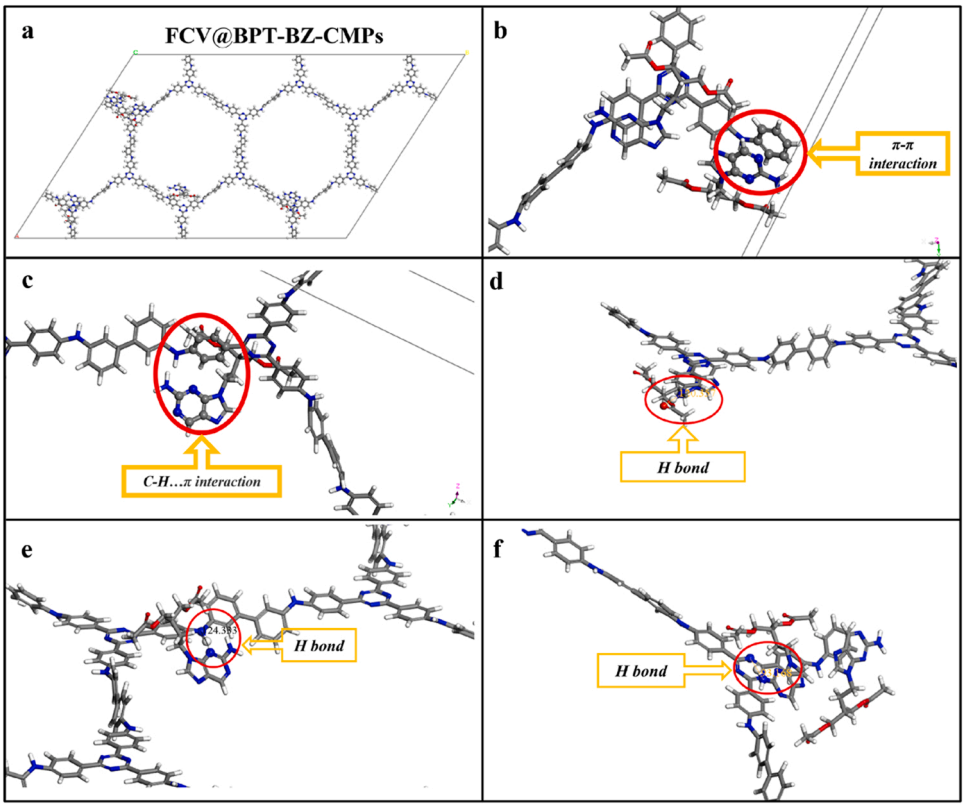

Fig. 9. Five molecules of each FCV@ 3 × 2 × 1BPT-BZ-CMP unit cell configuration; FCV@ 3 × 2 × 1BPT-BZ-CMP (a); π–π interaction (b); C–H···π interaction (c) and H bond interaction (d, e and f) between the FCV@BPT-BZ-CMP system.

between the triazine or imino groups on BPT-BZ-CMP and the aromatic rings or carbonyl groups on FCV molecules (Fig. 9d–f). Thus, the enhanced adsorption behavior of BPT-BZ-CMP may be based on the following reasons. First, the π–π and C–H···π interactions formed between the benzene ring and C–H on BPT-BZ-CMP and the π-electron-rich aromatic ring of FCV strengthened the van der Waals force, therefore, the nonbonding interaction and the adsorption energy were enhanced. Second, the N–H···N and N–H···O hydrogen bond interactions between the triazine or imino groups on BPT-BZ-CMP and the aromatic rings or carbonyl groups on FCV molecules enhanced the intermolecular interactions. The binding energy of the FCV@BPT-BZ-CMP system (E_{bind}) was − 34.9 kcal·mol^{-1}. Additionally, the BPT-BZ-CMP with high surface area increased the adsorption sites and induced van der Waals interactions. Based on the aforementioned analysis of potential mechanisms, the theoretical explanations correlated with the experimental data in terms of the excellent FCV removal capacity of BPT-BZ-CMP.

4. Conclusions

In conclusion, BPT-BZ-CMP was synthesized by the BH coupling reaction and was applied firstly to remove FCV from an aqueous solution. The morphological characteristics of BPT-BZ-CMP were investigated by FT-IR, SEM, BET, XPS, and Zeta-potential analyses. The results showed that the solution pH of 6.0 and sorbent concentration of 0.50 g·L^{-1} were the optimal adsorption conditions. With its micropore structure and high specific surface area, BPT-BZ-CMP only required a short time (30 min) to reach the adsorption equilibrium for FCV, and the maximum adsorption capacity can reach 347.8 mg·g^{-1}. Meanwhile, the adsorption kinetics, isotherms, and thermodynamics of FCV onto BPT-BZ-CMP were studied. The results showed that the Liu and pseudo-second-order kinetic models fit the adsorption equilibrium and adsorption kinetic data well, respectively, and the adsorption was a spontaneous endothermic process. The hydrogen bonding, π–π interaction and C–H···π interaction enhanced the adsorption of FCV on BPT-BZ-CMP. The adsorption capacity of BPT-BZ-CMP remained well after four consecutive adsorption–desorption cycles. This study provides a feasible method for the efficient and high-adsorption removal of FCV from the synthetic effluents of hospitals and pharmaceutical factories.

CRediT authorship contribution statement

Hai-Chen Tu: Data curation, Writing – original draft. **Ling-Xi Zhao:** Methodology, Writing – original draft. **Lu Liu:** Validation, Investigation. Xiao-Xing Wang: Investigation. **Jin-Ming Lin:** Supervision, Funding acquisition. **Xia Wang:** Writing – review & editing. **Ru-Song Zhao:** Conceptualization, Funding acquisition, Writing – editing.

Declaration of Competing Interest

The authors declare that they have no known competing financial interests or personal relationships that could have appeared to influence the work reported in this paper.

Data availability

Data will be made available on request.

Acknowledgment

This work was supported by National Natural Science Foundation of China (22076086), Shandong Province Taishan Scholar Program (ts20190948), Shandong Provincial Natural Science Foundation (ZR2022MB018), Project of Qilu University of Technology (Shandong Academy of Sciences) (2022PY027 and 2020KJC-ZD13), and Jinan University and Institute Innovation Team Project (2019GXRC032 and 2020GXRC008).

Appendix A. Supporting information

Supplementary data associated with this article can be found in the online version at doi:10.1016/j.colsurfa.2022.130393.

References

[1] K.G. Karthikeyan, M.T. Meyer, Occurrence of antibiotics in wastewater treatment facilities in Wisconsin, USA, Sci. Total Environ. 361 (2006) 196–207.
[2] F.D.L. Leusch, P.A. Neale, F. Busetti, M. Card, A. Humpage, J.D. Orbell, H. F. Ridgway, M.B. Stewart, J.P. van de Merwe, B.I. Escher, Transformation of endocrine disrupting chemicals, pharmaceutical and personal care products during drinking water disinfection, Sci. Total Environ. 657 (2019) 1480–1490.
[3] P.S. LaRussa, Famciclovir, Semin. Pedia Inf. Dis. 7 (1996) 138–144.
[4] F. Heidary, S. Madani, R. Gharebaghi, F. Asadi-amoli, Acyclovir as a potential adjuvant therapy in COVID-19 treatment regimens, Pharm. Sci. (2021).
[5] W.L. Chen, J.Y. Cheng, X.Q. Lin, Systematic screening and identification of the chlorinated transformation products of aromatic pharmaceuticals and personal care products using high-resolution mass spectrometry, Sci. Total Environ., 637-638 (2018) 253–263.
[6] S. Chen, Y. Wu, W. Zhang, S. Wang, T. Yan, S. He, B. Yang, H. Ma, A 3D ultramicroporous porous organic frameworks for SO2 and aromatic sulfides capture with high capacity and selectivity, Chem. Eng. J. 429 (2022).
[7] W. Zhang, Y. Li, S. Wang, Y. Wu, S. Chen, Y. Fu, W. Ma, Z. Zhang, H. Ma, Fluorine-Induced Electric Field Gradient in 3D Porous Aromatic Frameworks for Highly Efficient Capture of Xe and F-Gases, ACS Appl. Mater. Inter. 14 (2022) 35126–35137.
[8] W.L. Wang, Q.Y. Wu, Z.M. Wang, L.X. Niu, C. Wang, M.C. Sun, H.Y. Hu, Adsorption removal of antiviral drug oseltamivir and its metabolite oseltamivir carboxylate by carbon nanotubes: Effects of carbon nanotube properties and media, J. Environ. Manag. 162 (2015) 326–333.
[9] T.G. Kebede, M.B. Seroto, R.C. Chokwe, S. Dube, M.M. Nindi, Adsorption of antiretroviral (ARVs) and related drugs from environmental wastewaters using nanofibers, J. Environ. Chem. Eng. 8 (2020), 104049.
[10] S. Jain, R.K. Vyas, P. Pandit, A.K. Dalai, Adsorption of antiviral drug, acyclovir from aqueous solution on powdered activated charcoal: kinetics, equilibrium, and thermodynamic studies, Desalin. Water Treat. 52 (2013) 4953–4968.
[11] X. Bi, L.-X. Zhao, M. Xie, C. Zhang, J.-M. Lin, R.-S. Zhao, Functional metal–organic framework as high-performance adsorbent for selective enrichment of pharmaceutical contaminants in aqueous samples, Chem. Eng. J. 445 (2022), 136751.
[12] H. A.-s. Hosseini nasr, R. Akbarzadeh, Tayebee, Adsorption mechanism of different acyclovir concentrations on 1–2 nm sized magnetite nanoparticles: a molecular dynamics study, J. Mol. Liq. 254 (2018) 64–69.
[13] S. Han, D. Wu, S. Li, F. Zhang, X. Feng, Porous graphene materials for advanced electrochemical energy storage and conversion devices, Adv. Mater. 26 (2014) 849–864.
[14] M.G. Mohamed, S.V. Chaganti, M.-S. Li, M.M. Samy, S.U. Sharma, J.-T. Lee, M. H. Elsayed, H.-H. Chou, S.-W. Kuo, Ultrastable Porous Organic Polymers Containing Thianthrene and Pyrene Units as Organic Electrode Materials for Supercapacitors, ACS Appl. Energy Mater. 5 (2022) 6442–6452.
[15] M.G. Mohamed, W.-C. Chang, S.-W. Kuo, Crown Ether- and Benzoxazine-Linked Porous Organic Polymers Displaying Enhanced Metal Ion and CO_2 Capture through Solid-State Chemical Transformation, Macromolecules 55 (2022) 7879–7892.
[16] C. Hua, A. Rawal, T.B. Faust, P.D. Southon, R. Babarao, J.M. Hook, D. M. D'Alessandro, Exploiting stable radical states for multifunctional properties in triarylamine-based porous organic polymers, J. Mater. Chem. A 2 (2014) 12466–12474.
[17] R. Dawson, A.I. Cooper, D.J. Adams, Nanoporous organic polymer networks, Prog. Polym. Sci. 37 (2012) 530–563.
[18] K. Wang, H. Huang, D. Liu, C. Wang, J. Li, C. Zhong, Covalent Triazine-Based Frameworks with Ultramicropores and High Nitrogen Contents for Highly Selective CO_2 Capture, Environ. Sci. Technol. 50 (2016) 4869–4876.
[19] X. Liu, Y. Xu, D. Jiang, Conjugated microporous polymers as molecular sensing devices: microporous architecture enables rapid response and enhances sensitivity in fluorescence-on and fluorescence-off sensing, J. Am. Chem. Soc. 134 (2012) 8738–8741.
[20] W. Zhao, Y. Jiao, J. Li, L. Wu, A. Xie, W. Dong, One-pot synthesis of conjugated microporous polymers loaded with superfine nano-palladium and their micropore-confinement effect on heterogeneously catalytic reduction, J. Catal. 378 (2019) 42–50.
[21] M. Mohamed Samy, I.M.A. Mekhemer, M.G. Mohamed, M. Hammad Elsayed, K.-H. Lin, Y.-K. Chen, T.-L. Wu, H.-H. Chou, S.-W. Kuo, Conjugated microporous polymers incorporating Thiazolo[5,4-d]thiazole moieties for Sunlight-Driven hydrogen production from water, Chem. Eng. J. 446 (2022).
[22] Y. Kou, Y. Xu, Z. Guo, D. Jiang, Supercapacitive energy storage and electric power supply using an aza-fused pi-conjugated microporous framework, Angew. Chem. Int. Ed. Engl. 50 (2011) 8753–8757.
[23] J. Chen, T. Qiu, W. Yan, C.F.J. Faul, Exploiting Hansen solubility parameters to tune porosity and function in conjugated microporous polymers, J. Mater. Chem. A 8 (2020) 22657–22665.
[24] Y. Liao, H. Wang, M. Zhu, A. Thomas, Efficient supercapacitor energy storage using conjugated microporous polymer networks synthesized from buchwald-hartwig coupling, Adv. Mater. 30 (2018), e1705710.
[25] Y. Liao, J. Weber, B.M. Mills, Z. Ren, C.F.J. Faul, Highly efficient and reversible iodine capture in hexaphenylbenzene-based conjugated microporous polymers, Macromolecules 49 (2016) 6322–6333.
[26] J. Chen, W. Yan, E.J. Townsend, J. Feng, L. Pan, V. Del Angel Hernandez, C.F. J. Faul, Tunable surface area, porosity, and function in conjugated microporous polymers, Angew. Chem. Int. Ed. Engl. 58 (2019) 11715–11719.
[27] Y. Liao, J. Weber, C.F.J. Faul, Conjugated microporous polytriphenylamine networks, Chem. Commun. 50 (2014) 8002–8005.
[28] J. Yu, H. Feng, L. Tang, Y. Pang, J. Wang, J. Zou, Q. Xie, Y. Liu, C. Feng, J. Wang, Insight into the key factors in fast adsorption of organic pollutants by hierarchical porous biochar, J. Hazard. Mater. 403 (2021), 123610.
[29] T.C. Voice, W.J. Weber, Sorbent concentration effects in liquid/solid partitioning, Environ. Sci. Technol. 19 (1985) 789–796.
[30] G. Xu, B. Zhang, X. Wang, N. Li, L. Liu, J.M. Lin, R.S. Zhao, Nitrogen-doped flower-like porous carbon nanostructures for fast removal of sulfamethazine from water, Environ. Pollut. 255 (2019), 113229.
[31] Y.S. Ho, G. McKay, The kinetics of sorption of basic dyes from aqueous solution by sphagnum moss peat, Can. J. Chem. Eng. 76 (1998) 822–827.
[32] T.A. Khan, S.A. Chaudhry, I. Ali, Equilibrium uptake, isotherm and kinetic studies of Cd(II) adsorption onto iron oxide activated red mud from aqueous solution, J. Mol. Liq. 202 (2015) 165–175.
[33] W.J. Dai, P. Wu, D. Liu, J. Hu, Y. Cao, T.Z. Liu, C.P. Okoli, B. Wang, L. Li, Adsorption of Polycyclic Aromatic Hydrocarbons from aqueous solution by Organic Montmorillonite Sodium Alginate Nanocomposites, Chemosphere 251 (2020), 126074.
[34] P. Hadi, K.Y. Yeung, J. Barford, K.J. An, G. McKay, Significance of microporosity on the interaction of phenol with porous graphitic carbon, Chem. Eng. J. 269 (2015) 20–26.
[35] H. Xu, S. Zhu, M. Xia, F. Wang, Rapid and efficient removal of diclofenac sodium from aqueous solution via ternary core-shell CS@PANI@LDH composite: Experimental and adsorption mechanism study, J. Hazard. Mater. 402 (2021), 123815.
[36] L. Yang, Y. Feng, C. Wang, D. Fang, G. Yi, Z. Gao, P. Shao, C. Liu, X. Luo, S. Luo, Closed-loop regeneration of battery-grade FePO4 from lithium extraction slag of spent Li-ion batteries via phosphoric acid mixture selective leaching, Chem. Eng. J. 431 (2022).
[37] W. Hu, L. Yang, P. Shao, H. Shi, Z. Chang, D. Fang, Y. Wei, Y. Feng, Y. Huang, K. Yu, X. Luo, Proton Self-Enhanced Hydroxyl-Enriched Cerium Oxide for Effective Arsenic Extraction from Strongly Acidic Wastewater, Environ. Sci. Technol. 56 (2022) 10412–10422.
[38] I. Langmuir, The adsorption of gases on plane surfaces of glass, mica and platinumm, J. Am. Chem. Soc. 40 (1918) 1361–1403.
[39] P.S. Thue, M.A. Adebayo, E.C. Lima, J.M. Sieliechi, F.M. Machado, G.L. Dotto, J.C. P. Vaghetti, S.L.P. Dias, Preparation, characterization and application of microwave-assisted activated carbons from wood chips for removal of phenol from aqueous solution, J. Mol. Liq. 223 (2016) 1067–1080.
[40] Y. Lv, J. Ma, K. Liu, Y. Jiang, G. Yang, Y. Liu, C. Lin, X. Ye, Y. Shi, M. Liu, L. Chen, Rapid elimination of trace bisphenol pollutants with porous beta-cyclodextrin modified cellulose nanofibrous membrane in water: adsorption behavior and mechanism, J. Hazard. Mater. 403 (2021), 123666.
[41] M.A. Ahmad, N.K. Rahman, Equilibrium, kinetics and thermodynamic of Remazol Brilliant Orange 3R dye adsorption on coffee husk-based activated carbon, Chem. Eng. J. 170 (2011) 154–161.
[42] D.F. Caicedo, G.S. dos Reis, E.C. Lima, I.A.S. De Brum, P.S. Thue, B.G. Cazacliu, D. R. Lima, A.H. dos Santos, G.L. Dotto, Efficient adsorbent based on construction and demolition wastes functionalized with 3-aminopropyltriethoxysilane (APTES) for the removal ciprofloxacin from hospital synthetic effluents, J. Environ. Chem. Eng. 8 (2020), 103875.
[43] Y. Liu, Is the free energy change of adsorption correctly calculated? J. Chem. Eng. Data 54 (2009) 1981–1985.
[44] F. Zhang, Q. Jin, S.-W. Chan, Ceria nanoparticles: size, size Distrib., shape, J. Appl. Phys. 95 (2004) 4319–4326.
[45] M.H. Dehghani, A.H. Hassani, R.R. Karri, B. Younesi, M. Shayeghi, M. Salari, A. Zarei, M. Yousefi, Z. Heidarinejad, Process optimization and enhancement of pesticide adsorption by porous adsorbents by regression analysis and parametric modelling, Sci. Rep. 11 (2021) 11719.
[46] E.C. Lima, A. Hosseini-Bandegharaei, J.C. Moreno-Piraján, I. Anastopoulos, A critical review of the estimation of the thermodynamic parameters on adsorption equilibria. Wrong use of equilibrium constant in the Van't Hoof equation for calculation of thermodynamic parameters of adsorption, J. Mol. Liq. 273 (2019) 425–434.
[47] X.Q. He, Y.Y. Cui, C.X. Yang, Thiol-yne click postsynthesis of a sulfonate group-enriched magnetic microporous organic network for efficient extraction of benzimidazole fungicides, ACS Appl. Mater. Inter. 13 (2021) 39905–39914.
[48] D. Sompornpailin, C. Ratanatawanate, C. Sattayanon, S. Namuangruk, P. Punyapalakul, Selective adsorption mechanisms of pharmaceuticals on benzene-1,4-dicarboxylic acid-based MOFs: effects of a flexible framework, adsorptive interactions and the DFT study, Sci. Total Environ. 720 (2020), 137449.